

Imaging of radiation damage using complementary field ion microscopy and atom probe tomography

Michal Dagan^{a,*}, Luke R Hanna^a, Alan Xu^a, Steve G Roberts^{a,b}, George D W Smith^a, Baptiste Gault^a, Philip D Edmondson^{a,**}, Paul A J Bagot^a, Michael P Moody^a

^aDepartment of Materials, University of Oxford, Parks Road, Oxford, OX1 3PH, UK

^bCulham Centre for Fusion Energy, Culham Science Centre, Abingdon, OX14 3DB, UK

*Corresponding author: Tel: +441865283658, Email address: Michal.dagan@materials.ox.ac.uk

**Current address: Oak Ridge National Laboratory, One Bethel Valley Road, Oak Ridge, TN 378316140 USA

Abstract

Radiation damage in tungsten and a tungsten-tantalum alloy, both of relevance to nuclear fusion research, has been characterized using a combination of field ion microscopy (FIM) imaging and atom probe tomography (APT). While APT provides 3D analytical imaging with sub-nanometer resolution, FIM is capable of imaging the arrangements of single atoms on a crystal lattice and has the potential to provide insights into radiation induced crystal damage, all the way down to its smallest manifestation – a single vacancy. This paper demonstrates the strength of combining these characterization techniques. In ion implanted tungsten, it was found that atomic scale lattice damage is best imaged using FIM. In certain cases, APT reveals an identifiable imprint in the data via the segregation of solute and impurities and trajectory aberrations. In a W-5at.%Ta alloy, a combined APT-FIM study was able to determine the atomic distribution of tantalum inside the tungsten matrix. An indirect method was implemented to identify tantalum atoms inside the tungsten matrix in FIM images. By tracing irregularities in the evaporation sequence of atoms imaged with FIM, this method enables the benefit of FIM's atomic resolution in chemical distinction between the two species.

Key words: field ion microscopy, atom probe tomography, radiation damage, crystal defects, tungsten, tungsten-tantalum alloy

1 Introduction

Nuclear fission power currently provides over 11% of the world's electricity demands and allows reliable electricity production, with negligible CO₂ emissions [1]. As nuclear fusion becomes increasingly recognized as a potential alternative to fission, great efforts are being made worldwide towards developing nuclear fusion reactors. These are aimed to offer a secure source of energy with no production of greenhouse gases, no long-lived radioactive waste and almost unlimited fuel supplies. In particular, ITER, a major international effort to build a commercial reactor-scale

fusion device, is currently undergoing construction [2]. Both fission and fusion reactors operate in a highly aggressive environment of high temperatures and high doses of energetic neutrons [3]–[7]. Bombardment by neutrons, characteristic of these environments, initializes atomic scale changes in the microstructures of the materials inside the reactor. Primary mechanisms of such initial changes are either displacement of atoms from their lattice positions by neutron collisions [8], or the generation of hydrogen and helium through chemical transmutation reactions that cluster into bubbles leading to undesirable swelling of the matrix [7]. These initial atomic scale changes further develop into a variety of chemical and structural features [9], [10] which can ultimately undermine critical mechanical properties through phenomena such as radiation induced embrittlement [11], radiation hardening [12] and radiation induced clustering [10]. It is therefore crucial to fully understand mechanisms that are in operation from even the earliest stages of atomic scale damage. Such knowledge will allow the accurate evaluation of operational lifetime of the different components, and the development of new, sustainable materials towards internal components of nuclear reactors.

Atom probe tomography (APT) has been established over the past decades as a key technique for the characterization of radiation-induced nanoscale damage in materials for fission and fusion applications [13]. Among these, case studies include radiation-induced clustering in reactor pressure vessels (RPV) steels [14]–[16], particle stability and distribution of oxide particles in oxide dispersion strengthened steels (ODS) [17]–[19], helium bubble trapping at oxide particles in ODS steels [20] and surface oxidation processes of stainless steels [21] and zirconium alloys [22] in corrosive environment. With the rise to prominence of APT, the potential of its forerunner, field ion microscopy (FIM), has largely been overlooked. While APT has proven capabilities for the study of small scale radiation induced chemical changes, it lacks the necessary spatial resolution and detection efficiency to image individual sites on the crystal lattice and therefore struggles in the direct imaging of atomic scale crystal damage. FIM, on the other hand, is comparatively more limited in terms of analytical capabilities. However, it enables direct imaging of complete crystallographic arrangements of atoms on the surface of the sample and can therefore constitute as a highly beneficial complementary technique to APT.

FIM and APT are based upon the concept of field ionization and field evaporation respectively [23]. Both techniques require a very sharp needle-shaped specimen, held in an ultra-high vacuum chamber, and exploit the fact that an intense electric field can be generated at its apex by application of a DC voltage. In APT, high voltage/laser light pulses are superimposed on the standing DC voltage to trigger the field evaporation of atoms on the surface of the specimen, which are in turn projected onto a position-sensitive detector. Each hit on the detector can be directly related to the pulse responsible for the single corresponding field evaporation event, facilitating highly accurate time-of-flight measurements and hence chemical identification. In the final step an inverse projection algorithm, combined with the sequence of evaporation and an assumed model for specimen shape enable a 3D atom-by-atom reconstruction of the analyzed volume [24].

In the case of FIM, the analysis chamber also contains inert imaging gas atoms at a pressure of approximately 10^{-5} mbar. The gas atoms are polarized by the electric field and are drawn to the tip, forming an adsorbed layer of atoms on the surface. If the electric field is sufficiently high, gas atoms above the specimen are ionized and projected onto a phosphor screen, producing a highly magnified image of the surface of the specimen. A typical FIM image of a tungsten sample oriented along the [011] direction is presented in Figure 1b. Each spot in the image represents the position of an individual atom on the surface of the tip. Since more gas ions originate from the vicinity of

the most protruding atoms, these locations are preferentially imaged and a terrace pattern is formed. Ultimately, the FIM image represents an atomic resolution quasi-stereographic projection of the crystal. If the applied electric field is increased sufficiently, atoms from the specimen itself can be field evaporated from the surface. In this way the specimen can be probed in depth, atom-by-atom and layer-by-layer enabling characterization of the internal microstructure.

Ground-breaking FIM studies in the 1960s-1980s previously demonstrated the direct imaging of radiation-induced voids, dislocations, self-interstitials, and single vacancies in the crystal lattice and brought significant new insights to the full spatial characterization of radiation-induced depleted zones [25]–[30]. However, these studies all predated digital imaging. While in the meantime little has changed in terms of FIM instrumentation, the capacity to capture such images digitally presents an array of new possibilities in terms of data collection, and tailored data analysis.

In this study, we explore potential applications and data analysis techniques for both FIM and APT. Firstly, we demonstrate combined APT/FIM study of radiation-induced crystal damage in tungsten samples. Tungsten is considered as a prime candidate material for different plasma facing components of future fusion reactors due to its high melting point, high thermal conductivity, low expansion coefficient and low erosion rate [31]. In particular, tungsten is being investigated for the use in the divertor and the first wall protection layer for future Tokamak based fusion reactors including and going beyond ITER [11], [32], [33].

Furthermore, an un-irradiated W-5at.%Ta alloy (hereafter termed ‘W-5Ta’) was also studied, and FIM analysis was developed to achieve atomic scale mapping of the distribution of solute tantalum atoms inside the tungsten matrix. The characterization of tungsten-tantalum alloys is of particular interest for fusion reactors as tantalum is a product of tungsten transmutation. Under ITER conditions, simulations show that about 0.6 at% tantalum will be formed from pure tungsten over the first five years of operation of commercial reactors [34]. Previous studies of W-5Ta have shown increased hardness post ion-implantation [35]. A similar phenomenon in W-5at.%Re alloys was found to be the result of radiation-induced solute clustering revealed by APT [36], which could indicate a potential reason for currently unexplained measured increase in W-5Ta hardness. The W-5Ta alloy was chosen here to demonstrate an atomic scale spatial distribution FIM technique that will potentially allow the detection of early stage clustering in FIM, beyond the APT detection power.

Contributions from both FIM and APT approaches used here for the study of tungsten, and tungsten-tantalum alloys are compared and discussed as well as future directions for complementary characterization protocols for APT/FIM.

2 Materials and Experiment

Tungsten samples (purity level >99.9 at %) were electropolished in a 5%NaOH solution from a tungsten wire oriented along the [011] direction, into sharp needle-shaped specimens, with an estimated apex radius of less than 50 nm. To simulate displacement damage from neutron bombardment [37], [38], the electropolished-needle specimens were subject to various tungsten ion implantations to create displacement cascades in the crystal lattice at increasing levels of

damage. Ion implantation is a commonly used proxy to model the effects of neutron irradiation within material systems and is usually a safer and more cost effective approach. Importantly, under controlled temperature and radiation rate conditions, in a matter of hours, ion irradiation can be used to induce radiation damage profiles that are characteristic of that induced by exposure to many years of reactor operation. While the nature of the interaction with the lattice, and as a result the scattering cross section and the penetration depth, are different in the ionic and neutral cases, there is ongoing work to investigate the validity of this widely used approximation and to optimize its application. [39], [40]. However, for the current study, seeking to characterize the broadly defined regimes of low, medium and high levels of damage, the profile damage that is produced from ion implantation remains a good approximation.

Further, W-5Ta alloy samples were also prepared from a W-5Ta ingot (supplied by Plansee) produced via sintering prior to hot extrusion and forging. The alloy ingot was sectioned using electrical discharge machining and profiled steel block and silicon carbide paper into 0.3x0.3x15mm matchsticks and further shaped by electropolishing with a 5%NaOH solution into needle-shaped specimens.

All ion implantations were carried out at the Surrey National Ion Beam Centre, UK. Table 1 summarizes the implantation conditions of each of the samples tested. SRIM 2013(stopping range of ions in matter) software was used to convert fluence to displacement per atom (dpa) values using a displacement energy of 68eV [41].

Both the FIM and APT measurements were destructive to each analyzed specimen, exploiting field evaporation of constituent atoms from the surface to generate 3D information. Hence, separate samples had to be prepared for each characterization technique. Atom probe analyses were performed using a LEAP-3000X HR, in laser-mode at a temperature of 50 K, a pulse repetition rate of 200 kHz with an evaporation rate of 0.002 ions/pulse. FIM analyses were performed on a 3DAP-LAR device, at a temperature of 50 K, using voltage pulsing at a repetition rate of 100 kHz. Ultra-high purity helium was used as the imaging gas.

	Material	Implantation energy [MeV]	Implantation temperature [C]	damage level [dpa]
Sample 1	W	X	X	0
Sample 2	W	0.15	25	0.01
Sample 3	W	2	500	6
Sample 4	W	2	500	33
Sample 5	W-5Ta	X	X	0

Table 1:
Summary of tungsten ion irradiation conditions. X represents specimens that were un-irradiated.

3 Results and Discussion

3.1 APT and FIM of Self Ion Irradiation of Tungsten

Figure 1 represents results from the FIM and APT analyses of the un-irradiated control tungsten samples. As expected, the reconstructed APT data in Figure 1a suggests a homogenous distribution of tungsten atoms. A clear crystal structure can also be seen in the FIM image in Figure 1b, fully characteristic of an undamaged body-centered cubic (bcc) lattice.

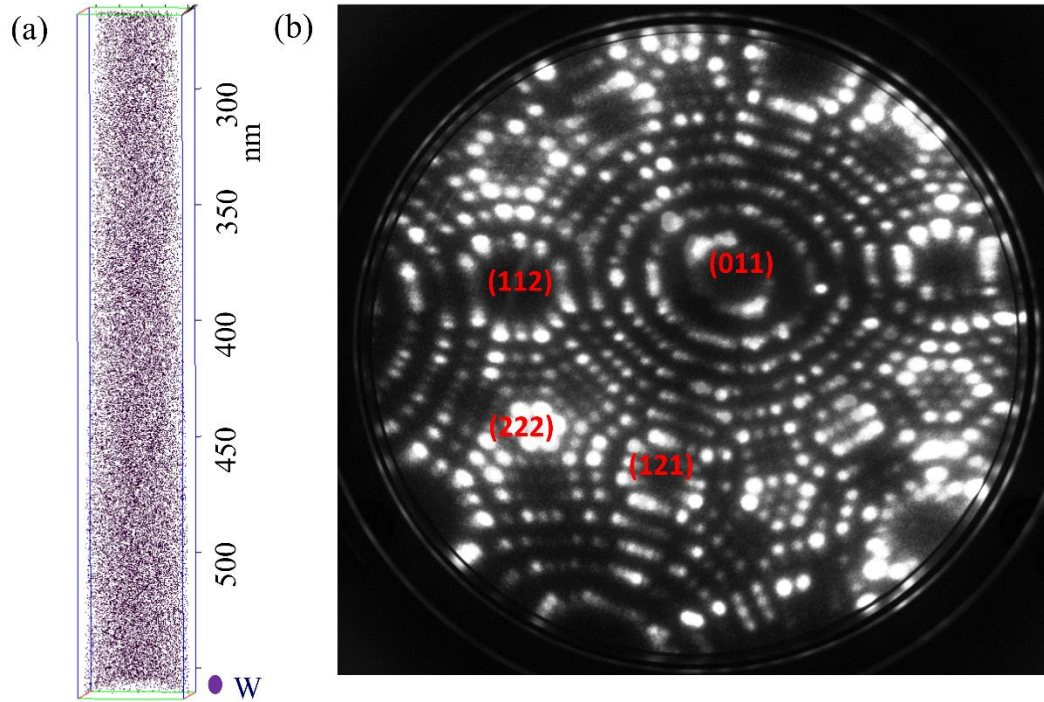


Figure 1 : APT and FIM results obtained for the reference un-implanted tungsten samples. (a) Homogenous tungsten matrix seen in the APT reconstruction. For clarity, 0.3% of the atoms are presented in a characteristic 300 nm long part of the reconstruction. (b) Characteristic bcc lattice imaged with FIM and helium as the imaging gas. Some of the main poles are indexed. Both measurements were taken at 50K.

It is only when comparing the results of the implanted samples to the reference samples that the differences in the relative strengths between the two techniques are made apparent. Figure 2 presents results of APT analyses of the samples implanted to a level of 0.01 dpa. The tungsten distribution within the APT reconstruction again appears homogenous, very similar to that in Figure 1a, with no significant indication of crystal damage caused by the implantation. However, by carefully examining the complementary FIM images in Figure 2 b-d, differences from the perfect crystal structure can be detected. Very fine features of crystal damage in the form of single vacancies can be seen throughout the evaporation process of the sample. These vacancies are straightforward to image with FIM, however are undetectable to APT analysis.

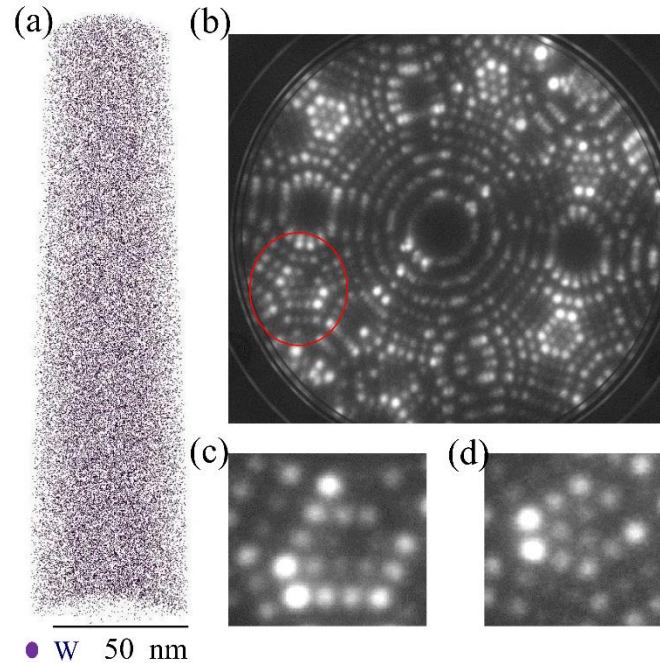


Figure 2 : Results from sample 2, tungsten implanted to a 0.01 dpa level. (a) Homogenous tungsten matrix seen in the APT reconstruction, similar to the reference sample. No lattice damage is detected. 0.2% of the atoms are shown for clarity. (b) FIM image very similar to the one in Figure 1b, but single vacancies can be seen throughout the evaporation (c,d) as a result from the implantation. Helium was used as the imaging gas for FIM. Both results were obtained at 50K.

Larger features of crystal damage are prominently visible via FIM analysis of the samples implanted to a higher damage level of 6 dpa, as shown in Figure 3d-e. The concentric ring structure defining the central (011) pole in Figure 1b has been replaced by a spiral (Figure 3d). This is clear evidence of a dislocation emerging from the (011) plane [42]. On examining the complementary APT reconstruction, in Figure 3a, the homogeneous distribution of tungsten atoms is once again very similar to that observed for the previous irradiation conditions, and provides no direct evidence of damage to the crystal lattice. Interestingly, however, in this sample, small amounts of carbon were also detected (0.13 at. %) in the APT analysis. Much smaller traces of carbon (<0.01 at %) were observed at the surface of the control specimen, whereas, the samples implanted to 6 and 33 dpa were found to contain increasing amounts of carbon (0.13-0.41 at % respectively). It is likely that this carbon is an unintentional impurity, due to ‘knock-in’ events occurring during the tungsten ion-implantation process. From the APT reconstruction of carbon atoms in the 6dpa sample (Figure 3b) it is apparent that this carbon impurity is in fact useful for revealing damage to the lattice that is not detectable from the examination of the tungsten atoms. Regions of high carbon concentrations are caused by segregation of carbon atoms into the vicinity of lattice defects. Indeed, the decoration of solutes facilitating the observation of crystallographic dislocations is well-established in the APT investigation of a wide variety of material systems [43]–[47]. Looking more closely at the distribution of tungsten atoms of the 6 dpa sample, there are regions of the data where the in-depth spatial resolution of the APT reconstruction is high enough to resolve ordered (011) crystallographic planes, as demonstrated in Figure 3c. In such regions a departure from the well-ordered planes structure can be observed in the vicinity of carbon atoms (marked as red spheres). This further strengthens the notion that the observed distribution of carbon correlates to

radiation induced lattice damage. The dislocations observed with the field ion microscope in the 6 dpa samples help to identify the defects seen in Figure 3b,c as dislocations. Smaller damaged regions in the size of several vacancies were also observed with FIM, but these are apparently too small to be highlighted by carbon segregation in the APT data.

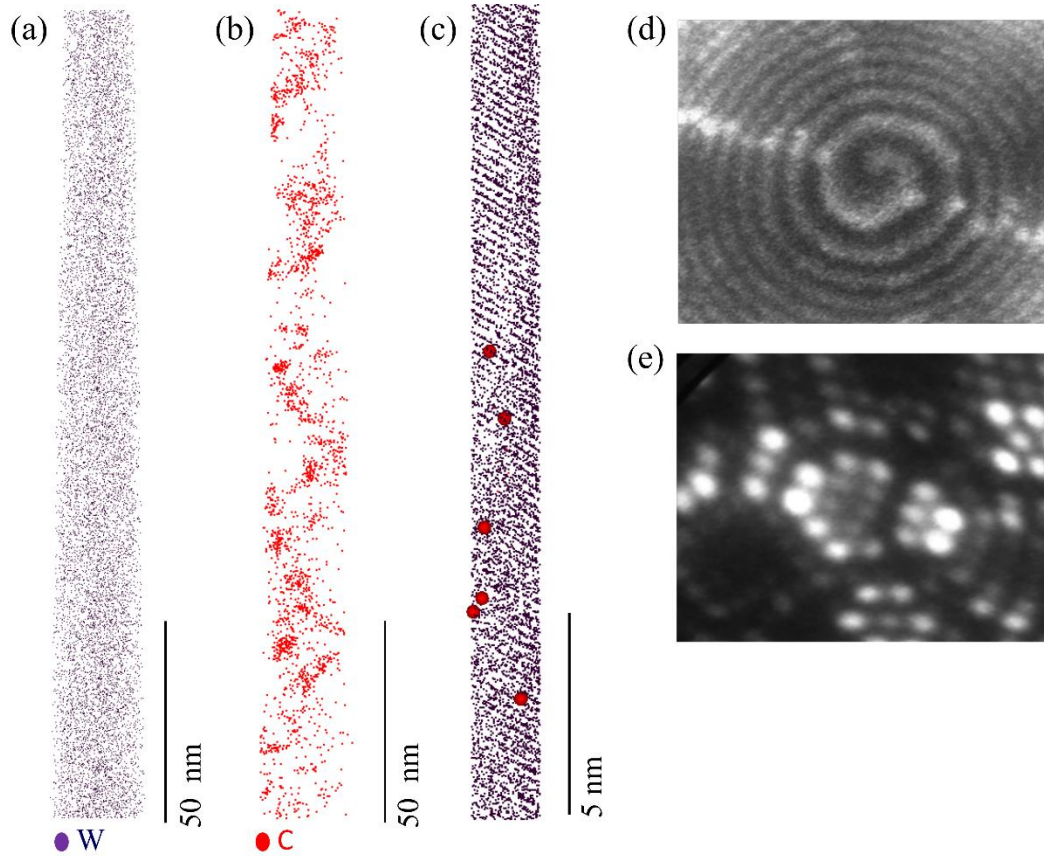


Figure 3 : Results from sample 3, tungsten implanted to a 6 dpa level, obtained at 50K (a) Tungsten APT reconstruction still appears to be homogenous with no apparent indication to crystal damage. For clarity, 1% of the atoms are shown here in a 200 nm long characteristic region. (b) APT reconstruction of carbon atoms present in the sample as a result of carbon contamination during tungsten ion implantation. Carbon segregates to damaged regions in the tungsten matrix and highlights them. The image shows the same region seen in 3a, with 100% of the carbon atoms. (c) A closer look into a 2x2x20 nm³ region of the tungsten matrix reveals (011) crystallographic planes. The carbon atoms in red are present at damaged regions of the planes. 85% of tungsten atoms are shown here for clear visualization of the planes. (d-e) FIM images presenting larger features of crystallographic damage than in previous samples. The spiral in d is a dislocation emerging from a (011) plane. Helium is used as the imaging gas.

It is only in the case of the highly damaged, 33 dpa sample, that the spatial distribution of tungsten in the APT reconstruction appears to be different from that of the corresponding control sample. Figure 4a exhibits high density regions in the tungsten reconstruction of the 33 dpa sample. These regions, highlighted by red circles in Figure 4a, can be attributed to trajectory aberrations in the atom probe caused by areas of lower curvature[48], [49]. Reports in the literature indicate that the field evaporation in defective areas, such as around dislocations [42], [50] or interstitials[51], occurs at lower electric field. Fortes and co-workers attribute a lower evaporation field to interstitial atoms due to the lattice strain[42]. The local neighborhood of these atoms is also likely to be affected by the binding energy of surface atoms in these areas[52], [53]. In addition, this is

supported by the carbon distribution in the sample, seen in Fig. 4b. The carbon exhibits segregation behavior similar to that observed in the 6 dpa sample and in many other materials, as recently reviewed by Smith et al.[54]. In this case, as seen in Figure 4 a-b, a correlation between carbon segregations and regions of tungsten high density is also revealed, further confirming the origin of the apparent high density tungsten regions as regions of extensive crystal damage. FIM images of sample 4 in Figure 4c-f reveal a considerably higher level of damage to the ordered lattice, with many dislocations, dislocation loops (Figure 4d) and depleted zones appearing throughout the evaporation process.

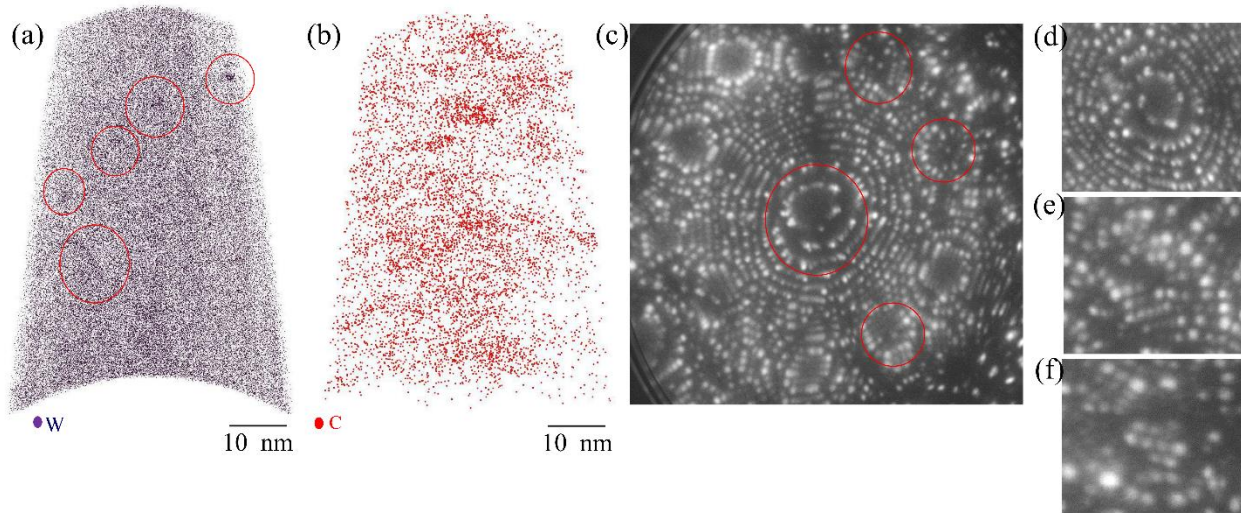


Figure 4 : Results from sample 4, tungsten implanted to a damage level of 33 dpa, taken at 50K. (a) Tungsten APT reconstruction reveals regions of high apparent density highlighted in red circles. For clarity, 80% of the atoms are shown in a $3.5 \times 50 \times 69 \text{ nm}^3$ slice of the data (b) Carbon segregation appear to spatially overlap with the high density tungsten regions. (c-f) FIM images presenting substantial degree of crystal damage. Helium is used as the imaging gas.

From the results described in Figures 1-4 it is clear that crystallographic information pertaining to radiation induced lattice damage is readily available in the FIM data. The atom probe data requires more careful analysis approaches and may not be successful in cases of low implantation levels where small features of damage are expected. It was shown that from the APT reconstructions of the tungsten matrix, no crystal damage was apparent up to a damage level of 6 dpa. At 33 dpa, large crystal defects manifested in the APT data in the form of density variations that can be attributed to trajectory aberrations.

The fundamental reason for this difference in resolution power lies with the use of imaging gas in FIM. In both FIM and APT, there is a random loss of 30-70% in detection efficiency due to the micro-channel plates (MCP) utilized at the entry of the detectors. In the case of a reflectron-fitted instrument such as the LEAP-3000HR used here, approximately 63% of the atoms evaporated from the specimen are stochastically omitted from the final analysis [55], [56]. Such limitations prevent the identification and characterization of atomic scale crystallographic features such as vacancies, interstitials, and the direct imaging of dislocations by the atom probe. However, the FIM image is dynamic, and is in fact the result of a continuous stream of gas ions field evaporated from the tip. At any given time each illuminated spot, representing an individual atom is made up from the contribution of thousands of gas ions striking the detector. Hence, even without the contribution of such a high proportion of imaging ions, the representation of specimen atoms in

FIM images is significantly increased in comparison to the atom probe. In regions of high index planes effectively every atom is precisely imaged on the lattice and consequently crystal defects, including the smallest of them all, the single vacancy, can be directly observed. This difference in detection and thus spatial resolution power is demonstrated in Figure 5. In Figure 5a, a simulation of the expected ion hit map around the main pole of APT data of a perfect bcc tip, aligned along the [011] direction. A concentric ring structure is obtained, representing the configuration of the kink sites, most prominent for evaporation, resulting from the intersection of the spherical shape of the tip with the crystal lattice. In Figure 5b, the ion hit map of a real tungsten data set is shown, constructed of a 10nm (in depth) layer of ions that hit the detector in the region of the (011) pole. The reduced detection efficiency and spatial resolution is immediately apparent. In comparison, Figure 5c shows a FIM image of a tungsten sample aligned at the same direction. The obvious concentric ring structure is very similar to the perfect crystal simulation, demonstrating the superior efficiency and resolution power of FIM vs the APT.

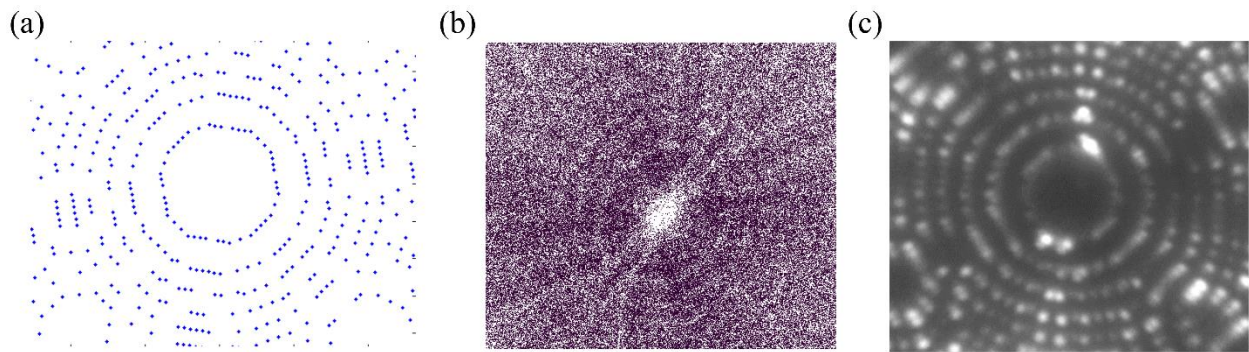


Figure 5 : FIM vs APT detection efficiency and spatial resolution comparison. (a) Simulation of the surface ion hit map around the (011) pole assuming 100% detection efficiency. (b) Ion hit map around the (011) pole of a real tungsten APT data set ran in voltage mode, constructed from a 10nm layer, 4-14 nms below the surface. (c) FIM image of the (011) pole of a tungsten tip, with helium as the imaging gas, taken at 50K, exhibiting periodic information on the crystal structure, in a similar manner to the simulation.

3.2 APT-FIM of W-5Ta

A tungsten sample and a W-5Ta alloy sample (both un-irradiated) were observed by FIM, and evaporation sequences of (222) planes were compared. Figure 6 shows results obtained from both samples. On the left, a typical evaporation sequence of tungsten (222) planes is shown. Images 1-9 in Figure 6a are time ordered. The most prominent atoms (those with the fewest nearest neighbours) are evaporated sequentially from outer terrace positions, one after the other. On the right, the evaporation sequence of (222) planes of the W-5Ta alloy is shown. Here, out of sequence evaporation events are detected, seen in the form of vacant sites at inner positions of the plane. Atoms in these positions had been evaporated prior to evaporation of kink atoms from the outer terrace.

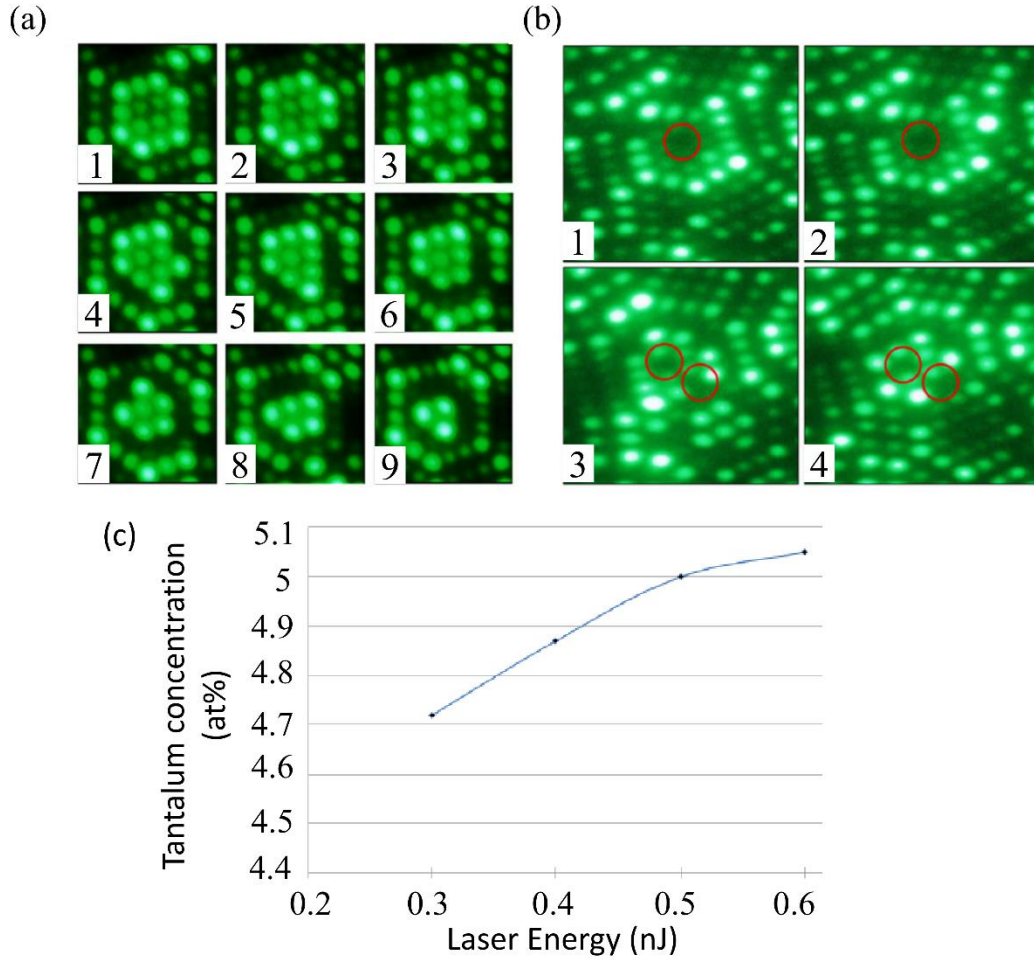


Figure 6 : (a) Typical (222) tungsten terrace evaporation sequence (b) out of sequence evaporation events in W-5Ta alloy highlighted in red circles. FIM measurements were taken at 30K with helium as the imaging gas (c) APT tantalum concentration measurements as a function of laser energy indicating preferential evaporation, taken at 50K.

As seen in Figure 6, out of sequence evaporation events were observed in a W-5Ta sample tested in the field ion microscope. These events were exploited here to identify tantalum atoms on FIM images, for the purpose of characterizing the spatial atomic scale distribution of tantalum atoms inside the tungsten matrix.

In the absence of time of flight measurements, the task of distinguishing between chemical species requires less direct approaches. Preferential evaporation can, in some cases, give rise to contrast variation in FIM images between matrix atoms and solute atoms [57]. In the case where the matrix is preferentially evaporated, the solute will be retained on the surface representing a highly localized region of very high curvature and field and hence these solutes will image more brightly. This has been used recently to image surface migration of carbon in steels during a FIM experiment [58]. In contrast, cases where solute atoms are preferentially evaporated will result in lower contrast representation of the solutes in FIM images, and, as is the case in Figure 6b, can sometimes appear as atoms missing from the FIM image altogether. In these cases, it is likely that for sufficiently large terraces, the evaporation field for edge tungsten atoms is higher than the evaporation field for tantalum atoms at centre sites of the plane. This results in preferential

evaporation of tantalum atoms from within the plane, also known as out of sequence evaporation events, deviating from the expected sequential evaporation of outer terrace atoms observed for tungsten, in Figure 6a. To support the assumption that tantalum preferential evaporation over tungsten is occurring in this case, APT measurements of tantalum concentration as a function of laser pulse fraction were performed. As seen in Figure 6c, the tantalum concentration measured is rising with increased laser pulse fraction until a plateau is reached. This rise can be explained by the evaporation of tantalum atoms under the high standing DC field, rather than by the laser pulses. This will result in an artificially lower tantalum concentration measure since all ions evaporated between pulses cannot be chemically identified but instead contribute simply noise in the APT mass spectrum. As the laser pulse fraction is increased, the standing voltage is automatically decreased to maintain a constant evaporation rate, until finally is no longer sufficient for the evaporation of tantalum atoms between laser pulses, and a plateau is reached in the measured tantalum concentration. This confirms the possibility of preferential evaporation of tantalum atoms over tungsten. In FIM, such preferential evaporation events can be exploited to identify sites of tantalum atoms, assessing the chemical identity in an indirect manner but with much higher sensitivity than in the APT.

Figure 7 shows the implementation of this technique on 6 consecutive (222) evaporated planes of W-5Ta. The lateral positions of the atoms on the planes were extracted from the FIM images (the depth coordinates are not scaled in the image, but are given by the evaporation order of the planes and crystallographic knowledge of the spacing between them). The faulty evaporations from within the inner sites of the planes are marked in red and are assumed to be tantalum atoms. Figure 7 is actually a 3D atomistic reconstruction of the evaporated volume of the (222) pole, and demonstrates the atomic scale distribution of tantalum atoms inside the tungsten matrix.

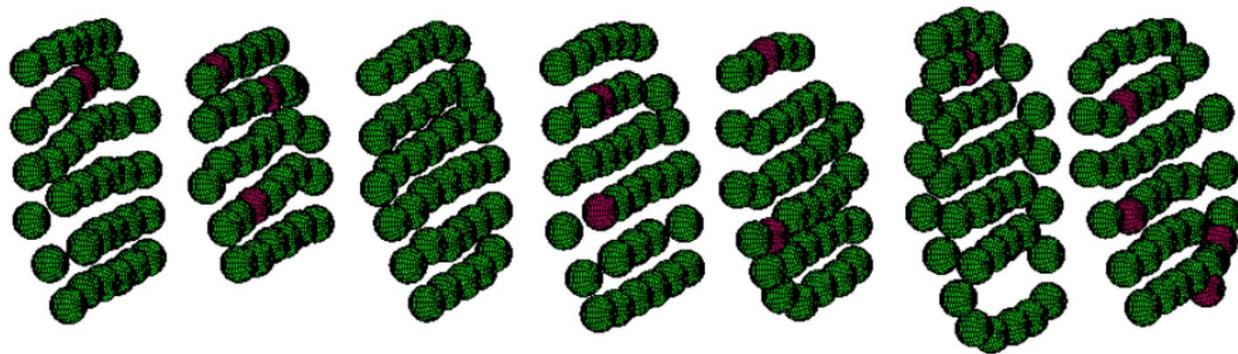


Figure 7 : Terrace reconstruction from FIM evaporation of 6 (222) planes in W-5Ta. Out of sequence evaporation events are marked in red and correspond to tantalum atoms, tungsten atoms marked in green.

The (222) pole was chosen for this analysis due to its clear atomic resolution and its potential for more highly controlled evaporation when compared to larger poles in the image. To verify that the determined tantalum distribution is representative of the bulk and not specifically characteristic of the (222) pole, 726 atoms corresponding to the evaporation of 20 (222) planes were evaporated. 38 atoms out of those were found to be out of sequence events and identified as tantalum atoms, making up 5.2 at.% out of the evaporated atoms. Although these are admittedly very small statistics, this number agrees with the expected composition which was verified by APT

measurements. This suggests no tantalum segregation to poles, confirming that the distribution of tantalum atoms in (222) planes is representative of the bulk structure.

However, when applying this method on implanted samples, additional caution must be taken. It was previously reported that faulty evaporation sequence events, of the type employed here to identify tantalum atoms, were also observed in irradiated materials in the vicinity of vacancies structures in (222) planes [59]. The presence of small vacancy defects can change the field distribution around neighboring atoms, and directly result in tungsten out of sequence evaporations such as the one seen on Figure 6b for W-5Ta. Therefore, when attempting to identify tantalum atoms in irradiated W-5Ta samples, where such defects are probable to occur, it is important to verify that there are no defects adjacent to those atoms suspected to be tantalum, otherwise, the origin of the faulty evaporation remains ambiguous. It is the highly controlled evaporation rate during the FIM run that allows the delicate distinction between a vacancy and an out of sequence evaporation event. Although both appear as vacant sites in the single FIM image, the out-of-sequence evaporated atom will be imaged in FIM images taken prior to its preferential removal, while the vacancy will not be imaged as an occupied site at any point in time.

4 Summary

Tungsten and tungsten-tantalum alloys have been studied to demonstrate the unique advantages of complementary atom probe and field ion microscopy analyses. It has been shown that the limits of both techniques can be further pushed by unconventional data mining efforts. FIM was found to be the preferred technique for the direct imaging of atomic scale lattice damage. While APT efficiency was proven to be insufficient for the direct imaging of such defects, indirect manifestation of these defects can appear in the APT data in the form of trajectory aberrations and decoration by impurities segregation. Further, it was shown that while FIM has no direct measures to distinguish between different chemical elements, out of sequence evaporation events can be employed for this purpose. It is therefore possible to exploit FIM's atomic resolution to characterize solute atom distribution inside a matrix on the atomic scale. Complementary atom probe data analysis has confirmed initial compositional results obtained by this technique.

The use of voltage pulsing enables controlled evaporation of specimen atoms in FIM which has the potential to underpin expansion of the technique from its historic role as atomistic surface technique, to 3D. With FIM's increased efficiency, a truly atomic scale 3D reconstruction of the crystal lattice is within reach as has been demonstrated in this work, however accurate and robust reconstruction protocols are in need of development to broaden the technique to larger volumes of analyzed data.

5 Acknowledgments

The authors would like to thank the UK's Engineering and Physical Sciences Research Council (EPSRC) for funding through the programme grant "Materials for Fission and Fusion Power" EP/H018921/1. PDE also acknowledges EPSRC support through a Career Acceleration Fellowship EP/K030043/1

BG acknowledges that he is a full time employee of Elsevier Ltd. but declares no conflict of interest as his contribution to this article corresponds to his activity out of office hours.

6 References:

- [1] "World Nuclear Association." [Online]. Available: <http://www.world-nuclear.org/info/Current-and-Future-Generation/Nuclear-Power-in-the-World-Today/>.
- [2] "ITER." [Online]. Available: <http://www.iter.org/>.
- [3] H. Bolt, V. Barabash, W. Krauss, J. Linke, R. Neu, S. Suzuki, and N. Yoshida, "Materials for the plasma-facing components of fusion reactors," *J. Nucl. Mater.*, vol. 329–333, pp. 66–73, Aug. 2004.
- [4] H. Bolt, V. Barabash, G. Federici, J. Linke, a Loarte, J. Roth, and K. Sato, "Plasma facing and high heat flux materials – needs for ITER and beyond," *J. Nucl. Mater.*, vol. 307–311, pp. 43–52, Dec. 2002.
- [5] S. J. Zinkle and J. T. Busby, "Structural materials for fission & fusion energy," *Mater. Today*, vol. 12, no. 11, pp. 12–19, Nov. 2009.
- [6] L. K. Mansur, A. F. Rowcliffe, R. K. Nanstad, S. J. Zinkle, W. R. Corwin, and R. E. Stoller, "Materials needs for fusion, Generation IV fission reactors and spallation neutron sources – similarities and differences," *J. Nucl. Mater.*, vol. 329–333, no. 2004, pp. 166–172, Aug. 2004.
- [7] G. Federici, C. H. Skinner, J. N. Brooks, J. P. Coad, C. Grisolia, A. A. Haasz, A. Hassanien, V. Philipps, C. S. Pitcher, J. Roth, W. R. Wampler, and D. G. Whyte, "Plasma-material interactions in current tokamaks," *Nucl. Fusion*, vol. 41, p. 1967, 2001.
- [8] G. H. Kinchin and R. S. Pease, "The displacement of atoms in solids by radiation," *Reports Prog. Phys.*, vol. 18, no. 1, pp. 1–51, Jan. 1955.
- [9] T. Diaz de la Rubia and M. W. Guinan, "New mechanism of defect production in metals: a molecular-dynamics study of interstitial-dislocation-loop formation in high energy displacement cascades," *Phys. Rev. Lett.*, vol. 66, no. 21, pp. 2766–2769, 1991.
- [10] T. Tanno, A. Hasegawa, J. C. He, M. Fujiwara, S. Nogami, M. Satou, T. Shishido, and K. Abe, "Effects of transmutation elements on neutron irradiation hardening of tungsten," *Mater. Trans.*, vol. 48, no. 9, pp. 2399–2402, 2007.
- [11] M. Rieth, S. L. Dudarev, S. M. Gonzalez de Vicente, J. Aktaa, T. Ahlgren, S. Antusch, D. E. J. Armstrong, M. Balden, N. Baluc, M.-F. Barthe, W. W. Basuki, M. Battabyal, C. S. Becquart, D. Blagoeva, H. Boldyryeva, J. Brinkmann, M. Celino, L. Ciupinski, J. B. Correia, A. De Backer, C. Domain, E. Gaganidze, C. García-Rosales, J. Gibson, M. R. Gilbert, S. Giusepponi, B. Gludovatz, H. Greuner, K. Heinola, T. Höschen, A. Hoffmann, N. Holstein, F. Koch, W. Krauss, H. Li, S. Lindig, J. Linke, C. Linsmeier, P. López-Ruiz, H. Maier, J. Matejicek, T. P. Mishra, M. Muhammed, A. Muñoz,

- M. Muzyk, K. Nordlund, D. Nguyen-Manh, J. Opschoor, N. Ordás, T. Palacios, G. Pintsuk, R. Pippin, J. Reiser, J. Riesch, S. G. Roberts, L. Romaner, M. Rosiński, M. Sanchez, W. Schulmeyer, H. Traxler, A. Ureña, J. G. van der Laan, L. Veleva, S. Wahlberg, M. Walter, T. Weber, T. Weitkamp, S. Wurster, M. A. Yar, J. H. You, and A. Zivelonghi, "Recent progress in research on tungsten materials for nuclear fusion applications in Europe," *J. Nucl. Mater.*, vol. 432, no. 1–3, pp. 482–500, Jan. 2013.
- [12] D. E. J. Armstrong, P. D. Edmondson, and S. G. Roberts, "Effects of sequential tungsten and helium ion implantation on nano-indentation hardness of tungsten," *Appl. Phys. Lett.*, vol. 102, no. 25, p. 251901, 2013.
- [13] E. A. Marquis, J. M. Hyde, D. W. Saxey, S. Lozano-Perez, V. de Castro, D. Hudson, C. A. Williams, S. Humphry-Baker, and G. D. W. Smith, "Nuclear reactor materials at the atomic scale," *Mater. Today*, vol. 12, no. 11, pp. 30–37, Nov. 2009.
- [14] M. K. Miller and K. F. Russell, "Embrittlement of RPV steels: An atom probe tomography perspective," *J. Nucl. Mater.*, vol. 371, no. 1–3, pp. 145–160, Sep. 2007.
- [15] P. Pareige, R. E. Stoller, K. F. Russell, and M. K. Miller, "Atom probe characterization of the microstructure of nuclear pressure vessel surveillance materials after neutron irradiation and after annealing treatments," vol. 249, no. 1997, pp. 165–174, 2008.
- [16] P. Auger, P. Pareige, S. Welzel, and J.-C. Van Duysen, "Synthesis of atom probe experiments on irradiation-induced solute segregation in French ferritic pressure vessel steels," *J. Nucl. Mater.*, vol. 280, no. 3, pp. 331–344, Aug. 2000.
- [17] M. K. Miller, E. A. Kenik, K. F. Russell, L. Heatherly, D. T. Hoelzer, and P. J. Maziasz, "Atom probe tomography of nanoscale particles in ODS ferritic alloys," vol. 353, no. 2003, pp. 140–145, 2008.
- [18] M. K. Miller, D. T. Hoelzer, E. A. Kenik, and K. F. Russell, "Nanometer scale precipitation in ferritic MA/ODS alloy MA957," *J. Nucl. Mater.*, vol. 329–333, no. 2004, pp. 338–341, Aug. 2004.
- [19] C. A. Williams, E. A. Marquis, A. Cerezo, and G. D. W. Smith, "Nanoscale characterisation of ODS–Eurofer 97 steel: An atom-probe tomography study," *J. Nucl. Mater.*, vol. 400, no. 1, pp. 37–45, May 2010.
- [20] P. D. Edmondson, C. M. Parish, Y. Zhang, a. Hallén, and M. K. Miller, "Helium entrapment in a nanostructured ferritic alloy," *Scr. Mater.*, vol. 65, no. 8, pp. 731–734, Oct. 2011.
- [21] S. Lozano-Perez, D. W. Saxey, T. Yamada, and T. Terachi, "Atom-probe tomography characterization of the oxidation of stainless steel," *Scr. Mater.*, vol. 62, no. 11, pp. 855–858, Jun. 2010.
- [22] D. Hudson, A. Cerezo, and G. D. W. Smith, "Zirconium oxidation on the atomic scale," *Ultramicroscopy*, vol. 109, no. 5, pp. 667–71, Apr. 2009.
- [23] B. Gault, M. P. Moody, J. M. Cairney, and S. P. Ringer, *Atom Probe Microscopy*. 2012.

- [24] F. Vurpillot, B. Gault, B. P. Geiser, and D. J. Larson, "Reconstructing atom probe data: a review.," *Ultramicroscopy*, vol. 132, pp. 19–30, Sep. 2013.
- [25] R. M. Scanlan, D. L. Styris, and D. N. Seidman, "An in situ field ion microscope study of irradiated tungsten," *Philos. Mag.*, vol. 23, no. 186, pp. 1439–1457, Jun. 1971.
- [26] M. Attardo and J. M. Galligan, "A field ion microscope study of neutron irradiated tungsten," *phys.stat.sol*, vol. 16, no. 2, pp. 449–457, 1966.
- [27] C. Y. Wei and D. N. Seidman, "Direct observation of the vacancy structure of depleted zones in tungsten ion irradiated at 10 K," *Appl. Phys. Lett.*, vol. 34, no. 10, p. 622, 1979.
- [28] D. N. Seidman, M. I. Current, D. Pramanik, and C. Y. Wei, "Direct observations of the primary state of radiation damage of ion-irradiated tungsten and platinum," *Nucl. Instruments Methods*, vol. 183, pp. 477–481, 1981.
- [29] D. N. Seidman, "The study of radiation damage in metals with the field ion and atom probe microscopes," *Surf. Sci.*, vol. 70, pp. 532–565, 1978.
- [30] C. Y. Wei, M. I. Current, and D. N. Seidman, "Direct observation of primary state of damage of ion-irradiated tungsten I. Three-dimensional spatial distribution of vacancies," *Philos. Mag. A*, pp. 459–491, 1981.
- [31] N. Yoshida, "Review of recent works in development and evaluation of high-Z plasma facing materials," *J. Nucl. Mater.*, vol. 266–269, pp. 197–206, Mar. 1999.
- [32] R. A. Pitts, S. Carpentier, F. Escourbiac, T. Hirai, V. Komarov, S. Lisgo, A. S. Kukushkin, A. Loarte, M. Merola, A. Sashala Naik, R. Mitteau, M. Sugihara, B. Bazylev, and P. C. Stangeby, "A full tungsten divertor for ITER: Physics issues and design status," *J. Nucl. Mater.*, vol. 438, pp. S48–S56, Jul. 2013.
- [33] V. Philipps, "Tungsten as material for plasma-facing components in fusion devices," *J. Nucl. Mater.*, vol. 415, no. 1, pp. S2–S9, Aug. 2011.
- [34] M. R. Gilbert, S. L. Dudarev, S. Zheng, L. W. Packer, and J. C. Sublet, "An integrated model for materials in a fusion power plant: transmutation, gas production, and helium embrittlement under neutron irradiation," *Nucl. Fusion*, vol. 52, no. 8, p. 083019, Aug. 2012.
- [35] D. E. J. Armstrong, A. J. Wilkinson, and S. G. Roberts, "Mechanical properties of ion-implanted tungsten–5 wt% tantalum," *Phys. Scr.*, vol. T145, p. 014076, Dec. 2011.
- [36] D. E. J. Armstrong, X. Yi, E. A. Marquis, and S. G. Roberts, "Hardening of self ion implanted tungsten and tungsten 5-wt% rhenium," *J. Nucl. Mater.*, vol. 432, no. 1–3, pp. 428–436, Jan. 2013.
- [37] S. J. Zinkle and A. Möslang, "Evaluation of irradiation facility options for fusion materials research and development," *Fusion Eng. Des.*, vol. 88, no. 6–8, pp. 472–482, Oct. 2013.

- [38] N. H. Packan, K. Farrell, and J. O. Stiegler, "Correlation of neutron and heavy-ion damage," *J. Nucl. Mater.*, vol. 78, pp. 143–155, 1978.
- [39] D. J. Mazey, S. Nelson, and J. A. Hudson, "The use of ion accelerators to simulate fast neutron-induced," vol. 37, pp. 1–12, 1970.
- [40] G. S. Was, Z. Jiao, E. Getto, K. Sun, a. M. Monterrosa, S. a. Maloy, O. Anderoglu, B. H. Sencer, and M. Hackett, "Emulation of reactor irradiation damage using ion beams," *Scr. Mater.*, vol. 88, pp. 33–36, Oct. 2014.
- [41] F. Maury, M. Biget, P. Vajda, A. Lucasson, and P. Lucasson, "Frenkel pair creation and stage I recovery in W crystals irradiated near threshold," *Radiat. Eff.*, vol. 38, no. 1–2, pp. 53–65, Jan. 1978.
- [42] M. A. Fortes, D. A. Smith, and B. Ralph, "The interpretation of field-ion micrographs: Contrast from perfect dislocation loops," *Philos. Mag.*, vol. 17, no. 145, pp. 169–176, Jan. 1968.
- [43] D. Blavette, E. Cadel, A. Fraczkiewicz, and A. Menand, "Three-dimensional atomic-scale imaging of impurity segregation to line defects," *Science (80-.)*, vol. 286, no. 5448, pp. 2317–2319, Dec. 1999.
- [44] K. Thompson, P. L. Flaitz, P. Ronsheim, D. J. Larson, and T. F. Kelly, "Imaging of arsenic Cottrell atmospheres around silicon defects by three-dimensional atom probe tomography," *Science*, vol. 317, no. 5843, pp. 1370–4, Sep. 2007.
- [45] M. K. Miller, "Atom probe tomography characterization of solute segregation to dislocations," *Microsc. Res. Tech.*, vol. 69, no. 5, pp. 359–65, May 2006.
- [46] M. Bachhav, L. Yao, G. Robert Odette, and E. A. Marquis, "Microstructural changes in a neutron-irradiated Fe–6at.%Cr alloy," *J. Nucl. Mater.*, Jul. 2014.
- [47] E. A. Marquis, M. Bachhav, Y. Chen, Y. Dong, L. M. Gordon, and A. McFarland, "On the current role of atom probe tomography in materials characterization and materials science," *Curr. Opin. Solid State Mater. Sci.*, vol. 17, no. 5, pp. 217–223, Oct. 2013.
- [48] F. Vurpillot, A. Bostel, and D. Blavette, "Trajectory overlaps and local magnification in three-dimensional atom probe," *Appl. Phys. Lett.*, vol. 76, no. 21, pp. 3127–3129, 2000.
- [49] M. K. Miller and M. G. Hetherington, "Local magnification effects in the atom probe," *Surf. Sci.*, vol. 246, pp. 442–449, 1991.
- [50] K. Hoummada, D. Mangelinck, B. Gault, and M. Cabié, "Nickel segregation on dislocation loops in implanted silicon," *Scr. Mater.*, vol. 64, no. 5, pp. 378–381, Mar. 2011.
- [51] M. J. Attardo and J. M. Galligan, "Radiation damage in platinum," *Phys. Rev. Lett.*, vol. 14, no. 16, p. 641, 1965.

- [52] A. J. W. Moore and J. A. Spink, "Field evaporation from tungsten and the bonding of surface atoms," *Surf. Sci.*, vol. 12, pp. 479–496, 1968.
- [53] X. Ge, N. Chen, W. Zhang, and F. Zhu, "Selective field evaporation in field-ion microscopy for ordered alloys," *J. Appl. Phys.*, vol. 85, no. 7, p. 3488, 1999.
- [54] G. D. W. Smith, D. Hudson, P. D. Styman, and C. A. Williams, "Studies of dislocations by field ion microscopy and atom probe tomography," *Philos. Mag.*, vol. 93, no. 28–30, pp. 3726–3740, Sep. 2013.
- [55] M. K. Miller, T. F. Kelly, K. Rajan, and S. P. Ringer, "The future of atom probe tomography," *Mater. Today*, vol. 15, no. 4, pp. 158–165, Apr. 2012.
- [56] T. F. Kelly and M. K. Miller, "Atom probe tomography," *Rev. Sci. Instrum.*, vol. 78, no. 3, p. 031101, Mar. 2007.
- [57] M. K. Miller, A. Cerezo, M. G. Hetherington, and G. D. W. Smith, *Atom probe field ion microscopy*. 1996.
- [58] B. Gault, F. Danoix, K. Hoummada, D. Mangelinck, and H. Leitner, "Impact of directional walk on atom probe microanalysis," *Ultramicroscopy*, vol. 113, pp. 182–191, Feb. 2012.
- [59] K. STILLER and H. O. Andren, "Faulty field evaporation at di-vacancies in {222} tungsten," *Surf. Sci.*, vol. 114, pp. 57–61, 1982.